

Symmetry-protected control of Liouvillian topological phases via Hamiltonian band topology

Shu Long,^{1,2} Chao Yang,³ Sen Mu,^{4,*} and Linhu Li^{1,†}

¹Quantum Science Center of Guangdong-Hong Kong-Macao Greater Bay Area (Guangdong), Shenzhen, China

²Guangdong Provincial Key Laboratory of Quantum Metrology and Sensing & School of Physics and Astronomy, Sun Yat-sen University (Zhuhai Campus), Zhuhai 519082, China

³Department of Physics, Southern University of Science and Technology, Shenzhen 518055, China

⁴Max Planck Institute for the Physics of Complex Systems, Nöthnitzer Str. 38, 01187 Dresden, Germany

We establish a symmetry-protected correspondence between band topology of coherent Hamiltonians and Liouvillian spectral winding in Lindblad descriptions of open quantum systems. This allows the Hamiltonian topology to act as a knob for controlling Liouvillian topology and corresponding non-equilibrium dynamics, rather than being passively manipulated by system-environment exchanges. In particular, by exactly solving the Liouvillian spectrum in a class of one-dimensional dissipative lattices, we find that the Hamiltonian band topology constrains the Liouvillian spectral winding and determines the Liouvillian skin effect, provided the Hamiltonian and quantum jump operators respect the same chiral symmetry. We further demonstrate that lattice parity controls the associated bulk-boundary correspondence and the coherence properties of the steady state. Our results unveil a symmetry-enforced topological control of spectral and spatial organization in open quantum systems, providing a unified perspective on topology in Hamiltonian and dissipative dynamics.

Introduction.— Open quantum systems can be described by the Lindbladian master equation, whose Liouvillian superoperator is intrinsically non-Hermitian and admits complex spectra absent in closed systems [1–9]. In particular, a new class of point-gap topological phases characterized by the spectral winding has recently been identified for such spectra [10–13]. This point-gap topology is closely connected to the Liouvillian skin effect (LSE), i.e., the accumulation of a macroscopic set of spatial decay modes near boundaries under open boundary conditions (OBC), potentially including the steady state [13–25].

Unlike Hamiltonian band topology, which is formulated with Bloch eigenstates and protected by global discrete symmetries [26–28], Liouvillian spectral topology is rooted in the complex spectrum of the full Liouvillian superoperator and depends on both coherent Hamiltonian dynamics and dissipative jump processes. The two notions of topology are therefore defined at fundamentally different levels, one in the pseudospin space for the Bloch vector manifold of a Hermitian band structure, the other in the complex plane for eigenvalues of a non-Hermitian operator. Whether these distinct topological structures can be incorporated into a unified framework remains an open question.

In this letter, we establish a symmetry-protected correspondence between Hamiltonian band topology and Liouvillian spectral topology in a class of one-dimensional dissipative lattices, through which the former serves as a knob for tuning the spectral and spatial organization of open quantum systems. We analytically demonstrate that a \mathbb{Z} -type winding topology of the Hamiltonian can be mapped onto a \mathbb{Z}_2 spectral topology of the Liouvillian spectrum, provided that the Hamiltonian and quantum jump operators respect the same chiral symmetry. Consequently, the LSE and its associated dynamical signatures can be predicted directly from the Hamiltonian topology, despite the fundamentally non-unitary nature of the Lindblad evolution. Furthermore, we show that spatial parity also plays a crucial role in ensuring the bulk-boundary corre-

spondence of Liouvillian spectral topology and in shaping the coherence structure of the topological LSE states. Our results establish a symmetry-protected bridge between Hamiltonian and Liouvillian topology, revealing a mechanism for controlling non-equilibrium dynamics of open quantum systems via Hamiltonian band topology.

Model and topological winding numbers.— We consider generic one-dimensional two-band models with chiral symmetry, described by the Hamiltonian

$$\hat{H} = \sum_{l=1}^L \sum_s J_s |a, l + s\rangle \langle b, l| + \text{h.c.}, \quad (1)$$

where l labels the unit cell, L is the system size, and $|s| < L$ denotes the range of hopping from pseudospin or sublattice b to a . The explicit symmetry condition will be introduced later. Within the Born-Markov approximation [29, 30], dynamics of an open system is described by the Lindbladian master equation [1, 2],

$$\frac{d\hat{\rho}}{dt} = -i[\hat{H}, \hat{\rho}] + \sum_p \left(\hat{D}_p \hat{\rho} \hat{D}_p^\dagger - \frac{1}{2} \{ \hat{D}_p^\dagger \hat{D}_p, \hat{\rho} \} \right) \equiv \mathcal{L}\hat{\rho}, \quad (2)$$

where $\hat{\rho}$ is the density matrix and \hat{D}_p are jump operators. We take linear dissipators of the form

$$\hat{D}_p \rightarrow \hat{D}_{l,s}^{\alpha,\alpha'} = \sqrt{\gamma_s^{\alpha,\alpha'}} |\alpha, l + s\rangle \langle \alpha', l| \quad (3)$$

with $\alpha, \alpha' \in \{a, b\}$, representing structured single-particle jump processes. The Liouvillian \mathcal{L} acts on the vectorized density matrix ρ in an extended Hilbert space of dimension $4L^2$ (see Supplemental Materials [31]), and satisfies $\mathcal{L}\rho_j = \lambda_j \rho_j$, where λ_j are the eigenvalues and ρ_j the corresponding normalized eigenmodes. The steady state is denoted by ρ_0 with $\lambda_0 = 0$, and the Liouvillian gap is defined as $\Delta\lambda = |\text{Re}[\lambda_1]|$ where $\text{Re}[\lambda_1] \geq \text{Re}[\lambda_j]$ for all $j \neq 0$.

By applying the Fourier transformation $|\alpha, l\rangle \langle \alpha', l'| = \frac{1}{L} \sum_{k,k'} e^{-ikl} e^{ik'l'} |\alpha, k\rangle \langle \alpha', k'|$, We obtain the Bloch form of the

Hamiltonian in Eq. (1),

$$H(k) = \begin{pmatrix} 0 & h^* \\ h & 0 \end{pmatrix} \quad (4)$$

with $h = \sum_{s=1}^{L-1} J_s e^{isk}$. The chiral symmetry reads

$$\{\sigma_z, H(k)\} = 0, \quad (5)$$

with σ_z acting in the pseudospin space. We can then define a winding number W_H characterizing the band topology of \hat{H} ,

$$W_H = \frac{1}{2\pi i} \int_0^{2\pi} dk \frac{d}{dk} \ln h. \quad (6)$$

By definition, W_H can take arbitrary integers, representing a \mathbb{Z} -type topology. Notably, each hopping term J_s contributes a winding number s , and the total winding can be viewed as a result of competition between Fourier harmonics in h .

For the Liouvillian superoperator \mathcal{L} in Eq. (2), although different quasi-momenta k and k' are coupled by the dissipative term $\hat{D}_{\rho\rho} \hat{D}_p^\dagger$, the momentum difference $K = k' - k$ labels an invariant subspace of the Liouvillian (see Supplemental Materials [31]). Thus, to describe the Liouvillian topology associated with the steady-state at $\lambda_0 = 0$, we define a spectral winding number for $\mathcal{L}(K)$ as

$$W_0 = \frac{1}{2\pi i} \int_0^{2\pi} dK \frac{d}{dK} \ln \det[\mathcal{L}(K) - 0^-], \quad (7)$$

which characterizes the winding of the Liouvillian spectrum near $\lambda = 0$. Given the established correspondence between the non-Hermitian skin effect and nontrivial spectral winding of non-Hermitian matrices [11, 12, 32], one expects the LSE of steady states to emerge whenever $W_0 \neq 0$. Note that W_0 is also a \mathbb{Z} -type topological invariant by definition; however, the spectral structure of the Liouvillian further enforces a \mathbb{Z}_2 topology with $W_0 = \pm 1$, as we will elaborate later.

Symmetry-protected topological imprint of the Hamiltonian onto Liouvillian spectral winding.— We aim to identify regimes where the topologies of the Hamiltonian and the Liouvillian can be captured by a symmetry-based framework. To achieve this, we consider dissipation that preserves the same chiral symmetry as the Hamiltonian in Eq. (5), $\{\sigma_z, \hat{D}_p\} = 0$. This condition restricts $\alpha' \neq \alpha$, and here we take $\alpha' = b$ and $\alpha = a$ without loss of generality. To clarify how the band topology of \hat{H} affects the Liouvillian spectral winding, we begin with a minimal Hamiltonian containing a single hopping term J_s at range $s = s_H$. This results in a winding number $W_H = s_H$, arising entirely from a single Fourier harmonic $h = e^{-is_H k}$ in Eq. (4). This case allows a transparent analytic treatment where the Hamiltonian band topology is cleanly imprinted onto the Liouvillian spectrum. In the following, we outline the main steps and results, while detailed derivations are provided in Supplemental Materials [31].

When the Hamiltonian is topologically trivial ($W_H = s_H = 0$), the Liouvillian superoperator admits an exact simplification in the basis of the vectorized density matrix,

$$\mathcal{L}(K) = I_L \otimes M + N_L \otimes M_0, \quad (8)$$

where I_L is the $L \times L$ identity matrix and N_L is an $L \times L$ matrix with all entries equal to one. The matrices M and M_0 are given explicitly by

$$M = \begin{pmatrix} 0 & iJ_0^* & -iJ_0 & 0 \\ iJ_0 & -B_4/2 & 0 & -iJ_0 \\ -iJ_0^* & 0 & -B_4/2 & iJ_0^* \\ 0 & -iJ_0^* & iJ_0 & -B_4 \end{pmatrix}, \quad M_0 = \begin{pmatrix} 0 & 0 & 0 & A_{14} \\ 0 & 0 & 0 & 0 \\ 0 & 0 & 0 & 0 \\ 0 & 0 & 0 & 0 \end{pmatrix}, \quad (9)$$

where $A_{14} = \sum_s \gamma_s^{a,b} e^{iKs}/L$, $B_4 = \sum_s \gamma_s^{a,b}$, and $A_{14}L = B_4$ when $K = 0$. Since $[I_L, N_L] = 0$, the eigenequation of $\mathcal{L}(K)$ can be solved analytically, giving rise to a single steady state ρ_0 with $\lambda_0 = 0$, determined by the characteristic equation $\det[\lambda - (M + M_0L)] = 0$ at $K = 0$. Its expansion near $K = 0$ yields $\lambda_0(K) \propto iK \sum_s s \gamma_s^{a,b}$, from which we deduce the point-gap winding [31]

$$W_0 = \text{Sgn}[\sum_s s \gamma_s^{a,b}], \quad (10)$$

representing a \mathbb{Z}_2 topology solely depending on the dissipation couplings.

We now consider the case where the Hamiltonian exhibits a nontrivial band winding number $W_H = s_H \neq 0$, generated by a single hopping term J_{s_H} . In this setting, the Liouvillian superoperator takes the form

$$\mathcal{L}(K) = \text{diag}[M_1, M_2, \dots, M_L] + N_L \otimes M_0, \quad (11)$$

where M_0 is the same as in Eq. (9), and M_n are given by

$$M_n = \begin{pmatrix} 0 & iJ_{s_H}^* e^{is_H k'_n} & -iJ_{s_H} e^{-is_H k_n} & 0 \\ iJ_{s_H} e^{-is_H k'_n} & -B_4/2 & 0 & -iJ_{s_H} e^{-is_H k_n} \\ -iJ_{s_H}^* e^{is_H k_n} & 0 & -B_4/2 & iJ_{s_H}^* e^{is_H k'_n} \\ 0 & -iJ_{s_H}^* e^{is_H k_n} & iJ_{s_H} e^{-is_H k'_n} & -B_4 \end{pmatrix} \quad (12)$$

with $k_n = 2n\pi/L$, $k'_n = K + k_n = K + 2n\pi/L$. We perform a gauge transformation that renders the spectral structure analytically tractable,

$$T_n^{-1} M_n T_n = M(J_0 \rightarrow J_{s_H}), \quad T_n^{-1} M_0 T_n = e^{-is_H K} M_0, \quad (13)$$

with $T_n = \text{diag}[e^{is_H K}, e^{-is_H k_n}, e^{is_H k'_n}, 1]$. This maps $\mathcal{L}(K)$ to the same structure as Eq. (8), with J_0 replaced by J_{s_H} and the phase factor in the dissipative term A_{14} shifted by $-s_H$. As a result, the expansion near $K = 0$ of the steady state yields $\lambda_0(K) \propto iK \sum_s (s - s_H) \gamma_s^{a,b}$, leading to the Liouvillian spectral winding number with the band winding number $W_H = s_H$ imprinted within,

$$W_0 = \text{Sgn}[\sum_s (s - s_H) \gamma_s^{a,b}]. \quad (14)$$

We emphasize that the Hamiltonian influences the Liouvillian winding W_0 solely through its topological winding number W_H , and not through the detailed hopping amplitude J_{s_H} . In short, when the jump operators preserve the same protecting symmetry as the Hamiltonian, the Hamiltonian topology is imprinted onto the Liouvillian spectral winding.

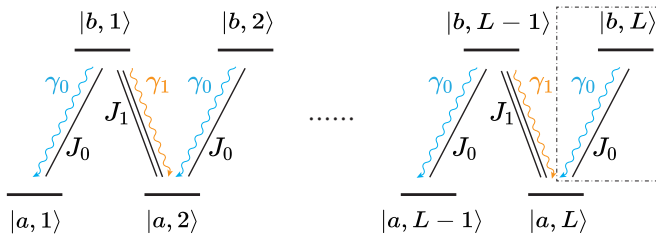


FIG. 1. Schematic of dissipative SSH model. J_0 (black single lines) and J_1 (black double lines) denote coherent hopping amplitudes. The blue and orange arrows represent two opposite dissipative couplings, γ_0 and γ_1 . Under OBC, their corresponding non-reciprocal dissipation channels are spatially balanced [i.e., satisfying the symmetry of Eq. (16)] in an edge-defect lattice with an edge site removed (e.g., $|b, L\rangle$ in the dashed box).

A dissipative Su-Schrieffer-Heeger model.— As a concrete example, we consider a dissipative extension of the Su-Schrieffer-Heeger (SSH) model [33], given by the Hamiltonian of Eq. (1) with nonzero J_0 and J_1 only, and two nearest-neighbor dissipative processes $\gamma_0^{a,b} \equiv \gamma_0$ and $\gamma_1^{a,b} \equiv \gamma_1$, as illustrated in Fig. 1. In the two limiting cases with $J_1 = 0$ or $J_0 = 0$, Eqs. (10) and (14) yield

$$W_0 = \begin{cases} \text{sgn}[\gamma_1] = 1, & \text{if } J_1 = 0 \\ -\text{sgn}[\gamma_0] = -1, & \text{if } J_0 = 0 \end{cases} \quad (15)$$

These two limits correspond to well-separated winding sectors of the Liouvillian spectrum. Beyond them, we note that the Liouvillian admits a symmetry under exchange of parameters between (J_0, γ_0) and (J_1, γ_1) ,

$$T^{-1} \mathcal{L}(K) T = \mathcal{L}(-K)_{(J_0, \gamma_0, k, k') \leftrightarrow (J_1, \gamma_1, -k, -k')}, \quad (16)$$

where $T = \text{diag}[T_1, T_2, \dots, T_L]$ is defined as in Eq. (13). This leads that W_0 , defined through spectral winding as K encircles the origin, changes sign under the exchange of parameters. Furthermore, the Liouvillian winding is independent of the detailed dissipation strengths with $\gamma_0, \gamma_1 > 0$ in the two limits of Eq. (15). Thus, the transition point of the Hamiltonian band topology, $J_0 = J_1$, is also expected to mark the topological transition of the Liouvillian winding number W_0 , enforcing an exact correspondence between them.

In Fig. 2(a1), we show numerical results of the Liouvillian and Hamiltonian winding numbers as functions of J_0 at fixed J_1 . Both exhibit a topological transition at $J_0 = J_1$. Under OBC, the system also undergoes a phase transition at this point, evidenced by the asymptotic closing of the Liouvillian gap with increasing system size, as shown in Fig. 2(a2). We present the full Liouvillian spectra under OBC for two illustrative cases in Figs. 2(b) and 2(c). In both cases, eigenvalues with large negative real parts $\text{Re}[\lambda] \ll 0$ exhibit mixing, but the topological features near $\lambda = 0$ remain clearly visible. The PBC spectrum forms a loop encircling the OBC spectrum, whose winding direction is consistent with nontrivial point-gap winding number W_0 . Under OBC, the steady state ρ_0 shows clear localization at left (right) edge when $W_0 = -1$

($W_0 = 1$), as depicted in Figs. 2(d) and 2(e). We further compute the average position of the diagonal density matrix elements to quantify this localization,

$$\bar{n} = \sum_n (n - n_0) \rho_{nm}, \quad \rho_{nm} = \langle n | \hat{\rho}_0 | m \rangle, \quad (17)$$

with $n_0 = (1 + 2L)/2$ and basis mapping $|a, l\rangle \equiv |n\rangle$ for $n = 2l - 1$ and $|b, l\rangle \equiv |n\rangle$ for $n = 2l$. As shown in Fig. 2(a3), the normalized displacement $\bar{n}/(L-0.5)$ switches sharply from -1 to 1 across the transition point $J_1 = J_0$, confirming the correspondence between LSE direction and Liouvillian spectral winding. Beyond static properties, we also probe the dynamics by initializing the system in a localized state at the center, $|\psi_{\text{ini}}\rangle = |a, L/2\rangle$. As shown in Figs. 2(f) and 2(g), the time evolution of the diagonal elements $\rho_{mm}(t)$ obtained from Eq. (2) shows a unidirectional drift toward the edge aligned with localization direction of steady states. This dynamical behavior offers an additional clear signature of the LSE, governed by the Hamiltonian band topology.

Coherent/incoherent LSE and parity effect.— We note that the opposite non-reciprocal channels, arising from the dissipative couplings γ_0 and γ_1 , are expected to determine the direction of the LSE. Yet their explicit magnitudes do not enter the topological winding numbers in Eq. (15). At first glance, this seems inconsistent with the anticipated topological correspondence underlying the LSE. To visualize this, in Fig. 3(a), we examine the average position \bar{n} of the OBC steady state, within the same topological phase characterized by $W_0 = -1$ ($J_0 < J_1$). As the system approaches the limit $J_0 \rightarrow 0$, the steady state consistently localizes toward the left edge, irrespective of the strength of the opposing dissipative channel γ_1 , in agreement with the predicted spectral winding. However, near the topological phase transition $J_0 = J_1$, a sufficiently large γ_1 ($\sim 10^1$) drives the steady state to localize toward the right edge, opposite to the direction dictated by the Liouvillian winding number. This deviation appears to violate the expected bulk-boundary correspondence: the spectral flow near $\lambda = 0$ remains clockwise in both regimes as shown in Figs. 3(c) and 3(d), however the boundary accumulation direction reverses.

The deviation between the winding number and steady-state localization can be understood from the competition between different dissipative pumping channels. Note that the spectral winding is defined under PBC, where left- and right-directed dissipation channels are balanced. However, the OBC breaks this balance by removing a rightward dissipation γ_1 , leading to distinct coherence structures and effective spatial support for steady states localized at opposite edges. Specifically, the leftward dissipative coupling γ_0 pumps a state to $|a, l\rangle$ with $l = 1, 2, \dots, L$, which span a L -site subspace that are indirectly coupled through the coherent coupling J_0 and J_1 . A sufficiently strong γ_0 therefore induces a coherent steady state localized toward the left edge [as in Fig. 2(d)]. On the other hand, in the absence of γ_0 , $|a, L\rangle$ is directly and coherently coupled to another site $|b, L\rangle$, enlarging the effective spatial support to a $(L + 1)$ -site subspace for the rightward LSE in-

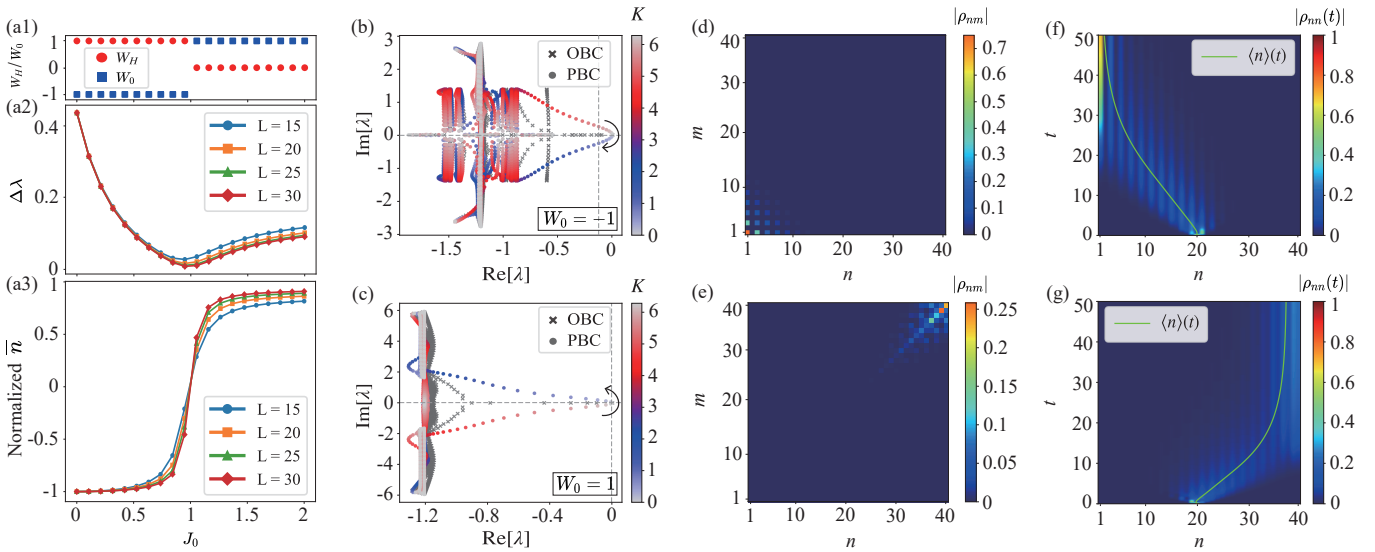


FIG. 2. (a) Topological transition of LSE characterized by the band winding number W_H [red dots in (a1)] and Liouvillian spectrum winding number W_0 [blue squares in (a1)]. Under OBC, the transition manifests as the closing of the Liouvillian gap $\Delta\lambda$ (a2) and the jump of normalized average position $\bar{n}/(L-0.5)$ of the steady state between -1 and 1 (a3), both are asymptotically achieved as the system size increases. (b) and (c) show the Liouvillian spectrum under OBC (gray) and PBC (colored). Colors represent different K values of the PBC eigenvalues. (d) and (e) the density matrix of the OBC steady-state $\hat{\rho}_0$ in (b) and (c), respectively. (f) and (g) time evolution of diagonal elements of the density matrix, ρ_{nn} , for an initial state $|\psi_{\text{ini}}\rangle = |a, L/2\rangle$. Green solid lines indicate the average position $\langle n \rangle = \sum_n n \rho_{nn}$. (b), (d), and (f) have $J_0 = 0.5$, and (c), (e), and (g) have $J_0 = 2$. Other parameters are $J_1 = 1$, $\gamma_0 = \gamma_1 = 1.2$, and $L = 20$.

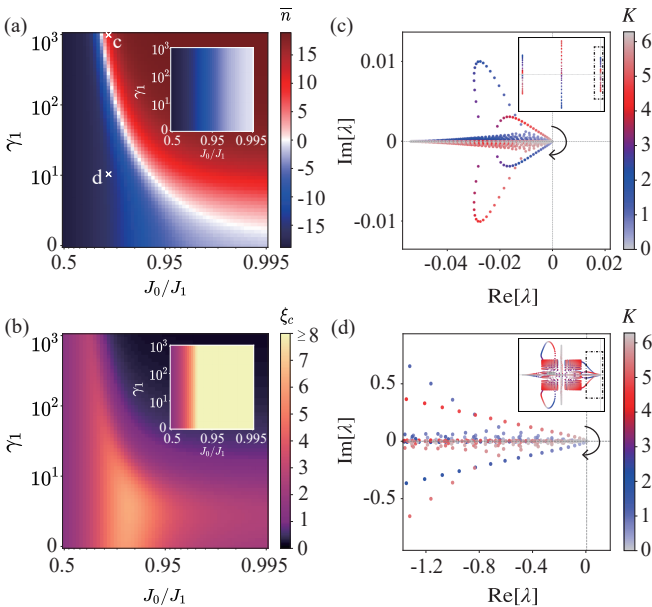


FIG. 3. (a) and (b) \bar{n} and ξ_c in logarithmic coordinates with $J_1 = 2$ and $\gamma_0 = 2$ under OBC. Insets show the same quantities for the edge-defect lattice with $|b, L\rangle$ removed [the system center in Eq. (17) becomes $n_0 = L$]. (c) and (d) the PBC spectra near $\lambda = 0$ for the two crosses marked in (a). The spectra show the same winding direction (clockwise), despite that the system possesses opposite edge localization in (a). Insets in (c) and (d) are the full Liouvillian spectra.

duced by γ_1 . The enlarged spatial support allows it to overwhelm the leftward pumping when $\gamma_1 \gg \gamma_0$. In addition, the

direct coherent coupling between $|a, L\rangle$ and $|b, L\rangle$ suppresses the indirect coherent couplings between $|a, l\rangle$, leading to an overall incoherent steady state [as in Fig. 2(e)].

To characterize the coherence behavior of steady state, we define a distance resolved coherence profile as

$$C(d) = \sum_l \sum_{\alpha, \alpha'} \langle \alpha, l | \rho_0 | \alpha', l+d \rangle. \quad (18)$$

By definition, $C(d > 0)$ is expected to decay faster than population decay for an incoherent state, and follow a systematic decay law tied to the localization length for a coherent state. Thus, we assume $C(d) \sim e^{-d/\xi_c}$ with a localization length as

$$\xi_c = 1 / \ln[C(0)/C(1)]. \quad (19)$$

As shown in Fig. 3(b), $\xi_c \approx 0$ in the regime with $\bar{n} > 0$, reflecting the decoherence of right-LSE. In the other regime with $\bar{n} < 0$, ξ_c generally takes a finite value, as the left-LSE steady state remains coherent. We further note that the left-LSE becomes more pronounced as J_0/J_1 decreases. In contrast, increasing J_0/J_1 enhances the competition from the rightward dissipative pumping channel γ_1 , which tends to suppress steady-state coherence. As a result, ξ_c attains its maximum at an intermediate value of J_0/J_1 , as can be seen in Fig. 3(b).

Finally, we emphasize that the decoherence of steady state and inconsistency between the Liouvillian winding number and steady state localization arise from the imbalance between the opposite pumping channels. Thus, we may remove an edge site to recover the balance in a lattice with an odd number of sites [see Fig. 1(a)], which resolves the inconsistency.

As shown in the insets of Figs. 3(a) and 3(b), both the steady-state position \bar{n} and the localization length ξ_c become insensitive to the strength of γ_1 , restoring an exact topological correspondence between the winding number and the LSE. In other words, the spatial parity essentially determines the balance between opposite pumping channels, and thus the exact topological correspondence of LSE.

Summary and discussion— We have analytically established a symmetry-protected correspondence between the Hamiltonian band topology and the Liouvillian spectral topology, as well as its further connection to the LSE, in Lindblad descriptions with the Hamiltonian and jump operators respecting the same chiral symmetry. The explicit correspondence is demonstrated in a prototypical model obeying the symmetry of Eq. (16) in parameter space; nonetheless, numerically we find that such correspondence remains valid even in the presence of long-range hoppings that breaks this parameter symmetry, as demonstrated in Supplemental Materials [31]. Besides, we note chiral-asymmetric dissipative processes can also lead to nontrivial W_0 and corresponding LSE. However, they are independent from the Hamiltonian band topology, as numerically demonstrated in the End Matter and analytically derived in Supplemental Materials [31]. Furthermore, we also reveal the crucial role of spatial parity in determining the exact correspondence between Liouvillian spectral winding and LSE. An extension with two hardcore bosons verifies the correspondence in the multi-particle scenario, as demonstrated in the end of Supplemental Materials [31]. These findings not only bridge the two distinct topological structures through symmetry protection, but also unveil the closed Hamiltonian topology as a governing principle and controlling method for the spectral and spatial organization of open quantum dynamics. Experimentally, the Hamiltonian and unidirectional dissipation in our model can be implemented with ultracold atoms in optical lattices [34–38], trapped-ion setups [39, 40] and superconducting qubits [41], offering a route for realizing topologically programmed steady states through our formalism.

Acknowledgment.— We acknowledge helpful discussion with Jiawei Zhang and Yu-Min Hu. This work is supported by the National Natural Science Foundation of China (Grant No. 12474159) and the Guangdong Provincial Quantum Science Strategic Initiative (Grant No. GDZX2504003 and GDZX2504006).

END MATTER

Chiral-asymmetric dissipation.— In the main text, we considered chiral-symmetric jump operators and demonstrated a close correspondence between band topology and Liouvillian spectral winding. To further elucidate the role of chiral symmetry in protecting this band-topology control of Liouvillian spectral winding and the LSE, we now introduce chiral-asymmetric dissipation terms $\gamma_s^{a,a} \equiv \gamma_1^{a,a}$ and $\gamma_s^{b,b} \equiv \gamma_{-1}^{b,b}$, i.e., $\{\sigma_z, \hat{D}_p\} \neq 0$, thereby explicitly breaking the protecting symmetry. In Fig. 4(a), we present the resulting phase dia-

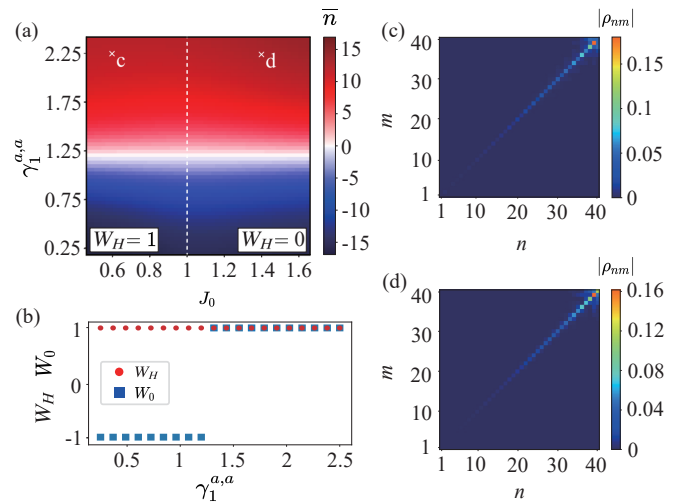


FIG. 4. Phase diagram and LSE with chiral-asymmetric dissipation. (a) The average position \bar{n} for different values of J_0 and $\gamma_1^{a,a}$. White dash line marks the transition of the band topology characterized by W_H . (b) Band winding number W_H (red dots) and Liouvillian spectrum winding number W_0 (blue squares) for different values of $\gamma_1^{a,a}$. (c) and (d) the density matrix of the OBC steady-state $\hat{\rho}_0$ with $J_0 = 0.6$ and $J_0 = 1.4$, respectively, marked by the white crosses in (a). The same localization direction is observed despite that they possess different W_H . Other parameters are $J_1 = 1$, $\gamma_{-1}^{b,b} = 1.2$, $L = 20$; and $\gamma_1^{a,a} = 2.25$ in (b) and (c).

gram under chiral-asymmetric dissipation. In stark contrast to the symmetric case, the band topology no longer controls the direction of the LSE; instead, the LSE direction is dictated solely by the relative strengths of the dissipative processes. Consistently, the Liouvillian spectral winding W_0 also becomes independent on the Hamiltonian winding W_H [Fig. 4(b)]. The steady-state density matrix $\hat{\rho}_0$ of two representative cases with different W_H are shown in Figs. 4(c) and (d), and both exhibit localization toward the same boundary, confirming the loss of topological correspondence. This behavior can be understood by noting that, under chiral-symmetric dissipation, the band topology effectively acts as a gauge field that modifies W_0 through a unitary transformation, thereby reversing the LSE direction. However, for the present asymmetric dissipation $\gamma_1^{a,a}$ and $\gamma_{-1}^{b,b}$, the winding information resides in diagonal components that are insensitive to this gauge structure (see Supplemental Materials [31]). Consequently, the Hamiltonian band topology no longer influences the direction of the LSE, underscoring that symmetry alignment is essential for the topological imprinting mechanism established in the main text.

Supplemental Materials

CONTENTS

I. Matrix form of the Liouvillian superoperator	6
A. Hamiltonian term	6
B. First term of jump operators	7
C. Second term of jump operators	8
II. The Liouvillian superoperator in momentum space	8
III. Exact solution of the Liouvillian spectrum in K -space with chiral-symmetric quantum jumps	9
A. $J_0 \neq 0, J_s = 0$	10
Solution of (i): Spectrum of M	10
Solution of (ii): Spectrum of $M + LM_0$	10
Total spectrum of $\mathcal{L}(K)$	11
Winding of the steady state	11
B. $J_0 = 0, J_s \neq 0$	12
C. The minimal model	13
IV. An example with chiral-symmetric quantum jumps and longer range hopping	13
V. Chiral-asymmetric quantum jumps	14
VI. The case of two hard-core bosons.	16
References	16

I. MATRIX FORM OF THE LIOUVILLIAN SUPEROPERATOR

In this section, we derive in detail the explicit expression for the corresponding Liouvillian superoperator after vectorizing the density matrix as

$$|\alpha, l\rangle\langle\alpha', l'| \rightarrow |\alpha, \alpha', l, l'\rangle. \quad (\text{S1})$$

For convenience, we derive the three terms in the Lindblad master equation of Eq.(2) in the main text separately.

A. Hamiltonian term

We first consider two-band systems with nontrivial topological properties protected by a chiral symmetry. The Hamiltonian is given by

$$\hat{H} = \sum_{l=1}^L \sum_{s=1-L}^{L-1} J_s |a, l+s\rangle\langle b, l| + \text{h.c.}, \quad (\text{S2})$$

The Hamiltonian term in the Liouvillian superoperator can be expressed as

$$\begin{aligned} \mathcal{L}_H(\hat{\rho}) &= -i[\hat{H}, \hat{\rho}] = -i \sum_{l, l'} \left([\hat{H}, |b, l\rangle\langle b, l'|] + [\hat{H}, |a, l\rangle\langle a, l'|] + [\hat{H}, |b, l\rangle\langle a, l'|] + [\hat{H}, |a, l\rangle\langle b, l'|] \right) \\ &= A + B + C + D, \end{aligned} \quad (\text{S3})$$

with

$$A = -i \sum_{l, l'} \left(\sum_{s=1-L}^{L-1} J_s |a, l+s\rangle\langle b, l'| - \sum_{s=1-L}^{L-1} J_s^* |b, l\rangle\langle a, l'+s| \right), \quad (\text{S4})$$

$$B = -i \sum_{l,l'} \left(\sum_{s=1-L}^{L-1} J_s^* |b, l-s\rangle \langle a, l'| - \sum_{s=1-L}^{L-1} J_s |a, l\rangle \langle b, l'-s| \right), \quad (\text{S5})$$

$$C = -i \sum_{l,l'} \left(\sum_{s=1-L}^{L-1} J_s |a, l+s\rangle \langle a, l'| - \sum_{s=1-L}^{L-1} J_s |b, l\rangle \langle b, l'-s| \right), \quad (\text{S6})$$

$$D = -i \sum_{l,l'} \left(\sum_{s=1-L}^{L-1} J_s^* |b, l-s\rangle \langle b, l'| - \sum_{s=1-L}^{L-1} J_s^* |a, l\rangle \langle a, l'+s| \right). \quad (\text{S7})$$

In the vector basis, these terms read:

$$\mathcal{L}_H |b, b, l, l'\rangle\rangle = -i \left(\sum_{s=1-L}^{L-1} J_s |a, b, l+s, l'\rangle\rangle - \sum_{s=1-L}^{L-1} J_s^* |b, a, l, l'+s\rangle\rangle \right), \quad (\text{S8})$$

$$\mathcal{L}_H |a, a, l, l'\rangle\rangle = -i \left(\sum_{s=1-L}^{L-1} J_s^* |b, a, l-s, l'\rangle\rangle - \sum_{s=1-L}^{L-1} J_s |a, b, l, l'-s\rangle\rangle \right), \quad (\text{S9})$$

$$\mathcal{L}_H |b, a, l, l'\rangle\rangle = -i \left(\sum_{s=1-L}^{L-1} J_s |a, a, l+s, l'\rangle\rangle - \sum_{s=1-L}^{L-1} J_s |b, b, l, l'-s\rangle\rangle \right), \quad (\text{S10})$$

$$\mathcal{L}_H |a, b, l, l'\rangle\rangle = -i \left(\sum_{s=1-L}^{L-1} J_s^* |b, b, l-s, l'\rangle\rangle - \sum_{s=1-L}^{L-1} J_s^* |a, a, l, l'+s\rangle\rangle \right). \quad (\text{S11})$$

Thus \mathcal{L}_H can be written as

$$\begin{aligned} \mathcal{L}_H = -i \sum_{l,l'} \left[\sum_{s=1-L}^{L-1} J_s \left(|a, b, l+s, l'\rangle \langle b, b, l, l'| + |a, a, l+s, l'\rangle \langle b, a, l, l'| \right. \right. \\ \left. \left. - |a, b, l, l'-s\rangle \langle a, a, l, l'| - |b, b, l, l'-s\rangle \langle b, a, l, l'| \right) + \text{h.c.} \right]. \end{aligned} \quad (\text{S12})$$

B. First term of jump operators

Consider the jump operators given by:

$$\hat{D}_{l,s}^{\alpha,\alpha'} = \sqrt{\gamma_s^{\alpha,\alpha'}} |\alpha, l+s\rangle \langle \alpha', l|. \quad (\text{S13})$$

The first quantum jump term in Eq.(2) is given by

$$\begin{aligned} \mathcal{L}_{D1}(\hat{\rho}) &= \sum_l \sum_{s,\alpha,\alpha'} \hat{D}_{l,s}^{\alpha,\alpha'} \hat{\rho} [\hat{D}_{l,s}^{\alpha,\alpha'}]^\dagger \\ &= \sum_l \sum_{s,\alpha,\alpha'} \gamma_s^{\alpha,\alpha'} |\alpha, l+s\rangle \langle \alpha', l| \hat{\rho} |\alpha', l\rangle \langle \alpha, l+s|, \end{aligned} \quad (\text{S14})$$

which leads to

$$\mathcal{L}_{D1} |\alpha', \alpha', l, l\rangle\rangle = \sum_{s,\alpha} \gamma_s^{\alpha,\alpha'} |\alpha, \alpha, l+s, l+s\rangle\rangle. \quad (\text{S15})$$

The operator can be written as

$$\mathcal{L}_{D1} = \sum_l \sum_{s,\alpha,\alpha'} \gamma_s^{\alpha,\alpha'} |\alpha, \alpha, l+s, l+s\rangle\rangle \langle\langle \alpha', \alpha', l, l|. \quad (\text{S16})$$

C. Second term of jump operators

According to Eq.(S13), the second term of the jump operators in Eq.(2) is:

$$\begin{aligned}\mathcal{L}_{D2}(\hat{\rho}) &= -\frac{1}{2} \sum_l \sum_{s,\alpha,\alpha'} \{[\hat{D}_{l,s}^{\alpha,\alpha'}]^\dagger \hat{D}_{l,s}^{\alpha,\alpha'}, \hat{\rho}\} \\ &= -\frac{1}{2} \sum_l \sum_{s,\alpha,\alpha'} \gamma_s^{\alpha,\alpha'} \{|\alpha', l\rangle\langle\alpha', l|, \hat{\rho}\}.\end{aligned}\quad (\text{S17})$$

Acting on different terms of the density matrix, we obtain

$$\mathcal{L}_{D2}|\alpha', \alpha', l, l'\rangle = -\sum_{s,\alpha} \gamma_s^{\alpha,\alpha'} |\alpha', \alpha', l, l'\rangle, \quad (\text{S18})$$

$$\mathcal{L}_{D2}|b, a, l, l'\rangle = -\frac{1}{2} \sum_{s,\alpha} \gamma_s^{\alpha,b} |b, a, l, l'\rangle - \frac{1}{2} \sum_{s,\alpha} \gamma_s^{\alpha,a} |b, a, l, l'\rangle, \quad (\text{S19})$$

$$\mathcal{L}_{D2}|a, b, l, l'\rangle = -\frac{1}{2} \sum_{s,\alpha} \gamma_s^{\alpha,a} |a, b, l, l'\rangle - \frac{1}{2} \sum_{s,\alpha} \gamma_s^{\alpha,b} |a, b, l, l'\rangle. \quad (\text{S20})$$

Thus the matrix form is given by

$$\begin{aligned}\mathcal{L}_{D2} &= -\sum_{l,l'} \left[\sum_{s,\alpha} \left(\gamma_s^{\alpha,b} |b, b, l, l'\rangle\langle\langle b, b, l, l'| + \gamma_s^{\alpha,a} |a, a, l, l'\rangle\langle\langle a, a, l, l'| \right) \right. \\ &\quad \left. + \frac{1}{2} \sum_{s,\alpha} \left(\gamma_s^{\alpha,b} + \gamma_s^{\alpha,a} \right) \left(|b, a, l, l'\rangle\langle\langle b, a, l, l'| + |a, b, l, l'\rangle\langle\langle a, b, l, l'| \right) \right],\end{aligned}\quad (\text{S21})$$

Combining Eq.(S12), Eq.(S16), and Eq.(S21) yields the matrix form of the Liouvillian superoperator in real space. Diagonalizing this matrix gives the Liouvillian spectrum and its eigenmodes.

II. THE LIOUVILLIAN SUPEROPERATOR IN MOMENTUM SPACE

After the Fourier transformation, Eq.(S12) can be written as

$$\begin{aligned}\mathcal{L}_H(k, k') &= -i \sum_{s=1-L}^{L-1} \left[J_s \left(e^{-isk} |a, b, k, k'\rangle\langle\langle b, b, k, k'| - e^{-isk'} |b, b, k, k'\rangle\langle\langle b, a, k, k'| \right. \right. \\ &\quad \left. \left. + e^{-isk} |a, a, k, k'\rangle\langle\langle b, a, k, k'| - e^{-isk'} |a, b, k, k'\rangle\langle\langle a, a, k, k'| \right) + \text{h.c.} \right].\end{aligned}\quad (\text{S22})$$

Its matrix form, with the basis arranged in the order of (aa, ab, ba, bb) , reads

$$\begin{pmatrix} 0 & iD_{k'}^* & -iC_k & 0 \\ iD_{k'} & 0 & 0 & -iC_k \\ -iC_k^* & 0 & 0 & iD_{k'}^* \\ 0 & -iC_k^* & iD_{k'} & 0 \end{pmatrix}, \quad (\text{S23})$$

with $C_k = \sum_{s=1-L}^{L-1} J_s e^{-isk}$, and $D_{k'} = \sum_{s=1-L}^{L-1} J_s e^{-isk'}$.

Eq.(S16)'s Bloch form after the transformation $|\alpha, \alpha', l, l'\rangle = \frac{1}{L} \sum_{k,k'} e^{-ikl} e^{ik'l'} |\alpha, \alpha', k, k'\rangle$ becomes more complicated:

$$\begin{aligned}\mathcal{L}_{D1}(k, k') &= \sum_{s,\alpha,\alpha'} \frac{\gamma_s^{\alpha,\alpha'}}{L^2} \sum_{k_1,k_1'} \sum_{k_2,k_2'} \sum_l e^{-i(k_1-k_1'-k_2+k_2')l} e^{-i(k_1-k_1')s} |\alpha, \alpha, k_1, k_1'\rangle\langle\langle\alpha', \alpha', k_2, k_2'| \\ &= \sum_{s,\alpha,\alpha'} \frac{\gamma_s^{\alpha,\alpha'}}{L} \sum_{k_1,k_1'} \sum_{k_2,k_2'} e^{-i(k_1-k_1')s} |\alpha, \alpha, k_1, k_1'\rangle\langle\langle\alpha', \alpha', k_2, k_2'| \delta_{k_1-k_1'-k_2+k_2'}.\end{aligned}\quad (\text{S24})$$

With these terms, different "momenta" are coupled together and no longer good quantum numbers, and we have to work in the subspace with constant $K = k' - k$. Its matrix form, with the basis arranged as (aa, ab, ba, bb) , reads

$$\begin{pmatrix} A_{11} & 0 & 0 & A_{14} \\ 0 & 0 & 0 & 0 \\ 0 & 0 & 0 & 0 \\ A_{41} & 0 & 0 & A_{44} \end{pmatrix}, \quad (\text{S25})$$

where $A_{11} = \sum_s \gamma_s^{\alpha,a} e^{iKs}/L$, $A_{14} = \sum_s \gamma_s^{\alpha,b} e^{iKs}/L$, $A_{41} = \sum_s \gamma_s^{b,a} e^{iKs}/L$, $A_{44} = \sum_s \gamma_s^{b,b} e^{iKs}/L$.

Applying the same transformation to Eq.(S21) yields:

$$\begin{aligned} \mathcal{L}_{D2}(k, k') = & - \left[\sum_{s,\alpha} \gamma_s^{\alpha,b} |b, b, k, k'\rangle \langle b, b, k, k'| + \sum_{s,\alpha} \gamma_s^{\alpha,a} |a, a, k, k'\rangle \langle a, a, k, k'| \right. \\ & \left. + \frac{1}{2} \sum_{s,\alpha} \left(\gamma_s^{\alpha,b} + \gamma_s^{\alpha,a} \right) \left(|b, a, k, k'\rangle \langle b, a, k, k'| + |a, b, k, k'\rangle \langle a, b, k, k'| \right) \right]. \end{aligned} \quad (\text{S26})$$

Thus the matrix form is given by

$$\begin{pmatrix} -\sum_{s,\alpha} \gamma_s^{\alpha,a} & 0 & 0 & 0 \\ 0 & -\frac{1}{2} \sum_{s,\alpha} \left(\gamma_s^{\alpha,b} + \gamma_s^{\alpha,a} \right) & 0 & 0 \\ 0 & 0 & -\frac{1}{2} \sum_{s,\alpha} \left(\gamma_s^{\alpha,b} + \gamma_s^{\alpha,a} \right) & 0 \\ 0 & 0 & 0 & -\sum_{s,\alpha} \gamma_s^{\alpha,b} \end{pmatrix}. \quad (\text{S27})$$

Based on Eq.(S23), Eq.(S25), and Eq.(S27), and since $K = k' - k$ is good quantum number, the Liouvillian superoperator in K -space takes the form

$$\mathcal{L}(K) = \text{diag}[M_1, M_2, \dots, M_L] + N_L \otimes M_0, \quad (\text{S28})$$

with N_L an $L \times L$ matrix with all elements being 1, and

$$M_n = \begin{pmatrix} -B_1 & iD_n^* & -iC_n & 0 \\ iD_n & -(B_1 + B_4)/2 & 0 & iC_n \\ -iC_n^* & 0 & -(B_1 + B_4)/2 & iD_n^* \\ 0 & -iC_n^* & iD_n & -B_4 \end{pmatrix}, \quad M_0 = \begin{pmatrix} A_{11} & 0 & 0 & A_{14} \\ 0 & 0 & 0 & 0 \\ 0 & 0 & 0 & 0 \\ A_{41} & 0 & 0 & A_{44} \end{pmatrix}. \quad (\text{S29})$$

The coefficients in Eq.(S29) are

$$\begin{aligned} A_{11} &= \sum_s \gamma_s^{\alpha,a} e^{iKs}/L, \quad A_{14} = \sum_s \gamma_s^{\alpha,b} e^{iKs}/L, \quad A_{41} = \sum_s \gamma_s^{b,a} e^{iKs}/L, \quad A_{44} = \sum_s \gamma_s^{b,b} e^{iKs}/L, \\ B_1 &= \sum_{s,\alpha} \gamma_s^{\alpha,a}, \quad B_4 = \sum_{s,\alpha} \gamma_s^{\alpha,b}, \\ C_n &= \sum_{s=1-L}^{L-1} J_s e^{-isk_n}, \quad D_n = \sum_{s=1-L}^{L-1} J_{s,+} e^{-isk'_n}, \end{aligned} \quad (\text{S30})$$

with $k_n = 2n\pi/L$ and $k'_n = K + k_n = K + 2n\pi/L$.

III. EXACT SOLUTION OF THE LIOUVILLIAN SPECTRUM IN K -SPACE WITH CHIRAL-SYMMETRIC QUANTUM JUMPS

We consider jump operators satisfying the same chiral symmetry as the Hamiltonian, i.e.,

$$\sigma_z \hat{D}_p \sigma_z = -\hat{D}_p. \quad (\text{S31})$$

This symmetry condition allows two classes of quantum jumps between different sublattices. Without loss of generality, in this subsection we consider the one from sublattice b to sublattice a .

$$\mathbf{A.} \quad J_0 \neq 0, J_s = 0$$

In this case, the Liouvillian superoperator can be further simplified into

$$\mathcal{L}(K) = I_L \otimes M + N_L \otimes M_0, \quad (\text{S32})$$

with $M = M_n$, as M_n becomes identical for different values of n . The matrix in Eq.(S32) are

$$M = \begin{pmatrix} 0 & iJ_0^* & -iJ_0 & 0 \\ iJ_0 & -B_4/2 & 0 & -iJ_0 \\ -iJ_0^* & 0 & -B_4/2 & iJ_0^* \\ 0 & -iJ_0^* & iJ_0 & -B_4 \end{pmatrix}, \quad M_0 = \begin{pmatrix} 0 & 0 & 0 & A_{14} \\ 0 & 0 & 0 & 0 \\ 0 & 0 & 0 & 0 \\ 0 & 0 & 0 & 0 \end{pmatrix}, \quad (\text{S33})$$

where $A_{14} = \sum_s \gamma_s^{a,b} e^{iKs}/L$, $B_4 = \sum_{s,\alpha} \gamma_s^{\alpha,b} = \sum_s \gamma_s^{a,b}$. Since I_L and N_L can be diagonalized and commute with each other, their action on the tensor product space spanned by the eigenvectors of N_L reduces $\mathcal{L}(K)$ into a direct sum of several 4×4 matrices. That is, as N_L has eigenvalues L (multiplicity 1) and 0 (multiplicity $L - 1$), the spectrum of $\mathcal{L}(K)$ is the union of:

- (i) Eigenvalues of M , each with multiplicity $L - 1$;
- (ii) Eigenvalues of $M + LM_0$, each with multiplicity 1.

Solution of (i): Spectrum of M

Assuming the eigenvalue of matrix M in Eq. (S33) is λ , its characteristic polynomial is:

$$P_M = \frac{1}{4}(2\lambda + B_4)^2(\lambda^2 + B_4\lambda + 4|J_0|^2). \quad (\text{S34})$$

Thus the eigenvalues of M are:

$$\lambda_1 = \lambda_2 = -\frac{B_4}{2}, \quad (\text{S35})$$

$$\lambda_3 = \frac{-B_4 \pm \sqrt{B_4^2 - 16|J_0|^2}}{2}. \quad (\text{S36})$$

Each of these eigenvalues appears in $\mathcal{L}(K)$ with multiplicity $(L - 1)$.

Solution of (ii): Spectrum of $M + LM_0$

Characteristic polynomial of $M + LM_0$ is:

$$P_{M+LM_0}(\lambda) = \frac{1}{4}(2\lambda + B_4) P_3(\lambda), \quad (\text{S37})$$

where

$$P_3(\lambda) = 2\lambda^3 + 3B_4\lambda^2 + (B_4^2 + 8|J_0|^2)\lambda + 4|J_0|^2(B_4 - A_{14}L). \quad (\text{S38})$$

Thus eigenvalues of $M + LM_0$ include:

$$\lambda = -\frac{B_4}{2}, \quad (\text{S39})$$

and the three roots of

$$\lambda^3 + \frac{3}{2}B_4\lambda^2 + \frac{B_4^2 + 8|J_0|^2}{2}\lambda + 2J_0^2(B_4 - A_{14}L) = 0. \quad (\text{S40})$$

Each of these eigenvalues appears in $\mathcal{L}(K)$ with multiplicity 1.

Total spectrum of $\mathcal{L}(K)$

Based on the solutions in Eqs.(S35), (S36), S39, S40 and their respective multiplicities, we obtain the spectrum of $\mathcal{L}(k)$ as:

$$\lambda = -\frac{B_4}{2} : \quad \text{multiplicity } (2L - 1), \quad (\text{S41})$$

$$\lambda = \frac{-B_4 \pm \sqrt{B_4^2 - 16|J_0|^2}}{2} : \quad \text{each multiplicity } L - 1, \quad (\text{S42})$$

and the three cubic roots of Eq. (S40), each appear with multiplicity 1.

Winding of the steady state

We note that physically we require both the Hamiltonian and quantum jump terms to be non-vanishing, i.e., $J_0 \neq 0$ and $B_4 \neq 0$. Thus, the only steady state is given by the simple root

$$\lambda_0 = 0 \quad (\text{S43})$$

of Eq. (S40) at $K = 0$ (so that $B_4 - A_{14}L = 0$). Next, upon tuning K slightly away from 0, we have

$$B_4 - A_{14}L = \sum_s \gamma_s^{a,b} (1 - e^{iKs}) \approx -i \sum_s s \gamma_s^{a,b} K. \quad (\text{S44})$$

Thus Eq. (S40) becomes

$$\lambda^3 + \frac{3}{2} B_4 \lambda^2 + \frac{B_4^2 + 8|J_0|^2}{2} \lambda - (2i|J_0|^2 \sum_s s \gamma_s^{a,b}) K = 0. \quad (\text{S45})$$

Dropping higher-order terms of $\lambda_0 \sim K$, the perturbed simple root $\lambda_0(K)$ satisfies

$$\begin{aligned} \lambda_0^3(K) + \frac{3}{2} B_4 \lambda_0^2(K) + \frac{B_4^2 + 8|J_0|^2}{2} \lambda_0(K) - (2i|J_0|^2 \sum_s s \gamma_s^{a,b}) K \\ \approx O(\lambda_0^2) + \frac{B_4^2 + 8|J_0|^2}{2} \lambda_0(K) - (2i|J_0|^2 \sum_s s \gamma_s^{a,b}) K = 0, \end{aligned} \quad (\text{S46})$$

$$\lambda_0(K) \approx \frac{4i|J_0|^2 \sum_s s \gamma_s^{a,b}}{B_4^2 + 8|J_0|^2} K. \quad (\text{S47})$$

Alternatively,

$$\lambda_0(K) = \lambda_0(0) - \frac{\partial P_3(\lambda = \lambda_0, K = 0)/\partial K}{\partial P_3(\lambda = \lambda_0, K = 0)/\partial \lambda} + O(K^2) \approx \frac{4i|J_0|^2 \sum_s s \gamma_s^{a,b}}{B_4^2 + 8|J_0|^2} K. \quad (\text{S48})$$

In addition, $\lambda_0(K \neq 0)$ correspond to non-steady states and have $\text{Re}[\lambda_0(K \neq 0)] < 0$. Therefore, the winding of the trajectory of $\lambda_0(K)$ near $K = 0$ depends on the sign of $\sum_s s \gamma_s^{a,b}$. Namely,

$$W_0 = \text{Sgn}[\sum_s s \gamma_s^{a,b}]. \quad (\text{S49})$$

Note that in principle W_0 cannot have magnitude larger than one, as it is defined for a negative real reference point which infinitely approaches $\lambda = 0$ from the negative direction of the real axis, and $\lambda_0 = 0$ has no degeneracy in our consideration. In this way, W_0 corresponds to the winding direction of the complex variant $B_4 - A_{14}L = \sum_s \gamma_s^{a,b} (1 - e^{iKs})$.

B. $J_0 = 0, J_s \neq 0$

Next we consider the case with non-trivial band topology produced by a single hopping parameter J_{s_0} . The corresponding Hamiltonian winding number is given by $W_H = s_0$. In this case, the Liouvillian becomes

$$\mathcal{L}(K) = \text{diag}[M_1, M_2, \dots, M_l] + N_L \otimes M_0, \quad (\text{S50})$$

where

$$M_n = \begin{pmatrix} 0 & iJ_{s_0}^* e^{is_0 k'_n} & -iJ_{s_0} e^{-is_0 k_n} & 0 \\ iJ_{s_0} e^{-is_0 k'_n} & -B_4/2 & 0 & -iJ_{s_0} e^{-is_0 k_n} \\ -iJ_{s_0}^* e^{is_0 k_n} & 0 & -B_4/2 & iJ_{s_0}^* e^{is_0 k'_n} \\ 0 & -iJ_{s_0}^* e^{is_0 k'_n} & iiJ_{s_0} e^{-is_0 k_n} & -B_4 \end{pmatrix}, \quad M_0 = \begin{pmatrix} 0 & 0 & 0 & A_{14} \\ 0 & 0 & 0 & 0 \\ 0 & 0 & 0 & 0 \\ 0 & 0 & 0 & 0 \end{pmatrix}, \quad (\text{S51})$$

with $A_{14} = \sum_s \gamma_s^{a,b} e^{iKs}/L$ and $B_4 = \sum_{s,\alpha} \gamma_s^{\alpha,b} = \sum_s \gamma_s^{a,b}$. To remove the n -dependence of M_n , we consider an alternative Fourier transformation,

$$|b, l\rangle = \frac{1}{\sqrt{L}} \sum_k e^{-ikl} |b, k\rangle, \quad |a, l\rangle = \frac{1}{\sqrt{L}} \sum_k e^{-ik(l-s_0)} |a, k\rangle. \quad (\text{S52})$$

Thus

$$|a, a, l, l'\rangle = \frac{1}{L} \sum_{k,k'} e^{-ikl} e^{ik'l'} e^{is_0 k} e^{-is_0 k'} |a, a, k, k'\rangle, \quad (\text{S53})$$

$$|a, b, l, l'\rangle = \frac{1}{L} \sum_{k,k'} e^{-ikl} e^{ik'l'} e^{is_0 k} |a, b, k, k'\rangle, \quad (\text{S54})$$

$$|b, a, l, l'\rangle = \frac{1}{L} \sum_{k,k'} e^{-ikl} e^{ik'l'} e^{-is_0 k'} |b, a, k, k'\rangle, \quad (\text{S55})$$

$$|b, b, l, l'\rangle = \frac{1}{L} \sum_{k,k'} e^{-ikl} e^{ik'l'} |b, b, k, k'\rangle. \quad (\text{S56})$$

It is equivalent to the following gauge transformation:

$$\begin{aligned} |a, a, k, k'\rangle &\rightarrow e^{is_0 k} e^{-is_0 k'} |a, a, k, k'\rangle, \\ |a, b, k, k'\rangle &\rightarrow e^{is_0 k} |a, b, k, k'\rangle, \\ |b, a, k, k'\rangle &\rightarrow e^{-is_0 k'} |b, a, k, k'\rangle, \\ |b, b, k, k'\rangle &\rightarrow |b, b, k, k'\rangle. \end{aligned} \quad (\text{S57})$$

Equivalently, the transformation matrix can be written as ($K = k' - k$)

$$T_n = \begin{pmatrix} e^{is_0 K} & 0 & 0 & 0 \\ 0 & e^{-is_0 k_n} & 0 & 0 \\ 0 & 0 & e^{is_0 k'_n} & 0 \\ 0 & 0 & 0 & 1 \end{pmatrix}, \quad (\text{S58})$$

so that

$$T_n^{-1} M_n T_n = M_{J_0 \leftrightarrow J_{s_0}}, \quad T_n^{-1} M_0 T_n = e^{-is_0 K} M_0. \quad (\text{S59})$$

Note that M_0 matrix also enters non-diagonal blocks. With these results, we can see that the case with $J_0 = 0$ and $J_{s_0} \neq 0$ can be mapped to the previous one with nonzero J_0 , with the coefficient A_{14} in M_0 matrix mapped to $e^{-is_0 K} A_{14}$. The steady state is still given by $\lambda_0 = 0$ at $K = 0$; however, upon slightly tuning away from $K = 0$, the perturbation term of Eq. (S44) becomes

$$B_4 - A_{14}L = \sum_s \gamma_s^{a,b} (1 - e^{iK(s-s_0)}) \approx -i \sum_s (s - s_0) \gamma_s^{a,b} K. \quad (\text{S60})$$

Thus, the Liouvillian spectral winding number becomes

$$W_0 = \text{Sgn}\left[\sum_s (s - s_0)\gamma_s^{a,b}\right]. \quad (\text{S61})$$

In other words, the Hamiltonian winding topology, characterized by the winding number $W_H = s_0$, modify the Liouvillian winding number through the complex variant $\sum_s \gamma_s^{a,b}(1 - e^{iK(s-s_0)})$.

C. The minimal model

We consider real nonzero parameters given by $J_0, J_1, \gamma_0^{a,b} \equiv \gamma_0$, and $\gamma_1^{a,b} \equiv \gamma_1$, which is the first explicit model we consider in the main text. In this case, many of the previous derivations can be further simplified. The matrices in Eq.(S32) are

$$M = \begin{pmatrix} 0 & iJ_0^* & -iJ_0 & 0 \\ iJ_0 & -B_4/2 & 0 & -iJ_0 \\ -iJ_0^* & 0 & -B_4/2 & iJ_0^* \\ 0 & -iJ_0^* & iJ_0 & -B_4 \end{pmatrix}, \quad M_0 = \begin{pmatrix} 0 & 0 & 0 & A_{14} \\ 0 & 0 & 0 & 0 \\ 0 & 0 & 0 & 0 \\ 0 & 0 & 0 & 0 \end{pmatrix}, \quad (\text{S62})$$

where $A_{14} = (\gamma_0 + \gamma_1)e^{iKs}/L$, $B_4 = \sum_{s,\alpha} \gamma_s^{\alpha,b} = \gamma_0 + \gamma_1$. Repeating the calculation above yields:

$$B_4 - A_{14}L = \gamma_1(1 - e^{iK}), \quad (\text{S63})$$

and the Liouvillian spectral winding is given by

$$W_0 = \text{Sgn}[\gamma_1] = 1. \quad (\text{S64})$$

For the case of non-trivial band topology, the matrices in Eq.(S32) become (here, $W_H = s_0 = 1$)

$$M_n = \begin{pmatrix} 0 & iJ_1 e^{ik'_n} & -iJ_1 e^{-ik_n} & 0 \\ iJ_1 e^{-ik'_n} & -B_4/2 & 0 & -iJ_1 e^{-ik_n} \\ -iJ_1 e^{ik_n} & 0 & -B_4/2 & iJ_1 e^{i0k'_n} \\ 0 & -iJ_1 e^{ik_n} & iJ_1 e^{-ik'_n} & -B_4 \end{pmatrix}, \quad M_0 = \begin{pmatrix} 0 & 0 & 0 & A_{14} \\ 0 & 0 & 0 & 0 \\ 0 & 0 & 0 & 0 \\ 0 & 0 & 0 & 0 \end{pmatrix}, \quad (\text{S65})$$

with $A_{14} = (\gamma_0 + \gamma_1)e^{iKs}/L$, $B_4 = \gamma_0 + \gamma_1$. Thus the transformation matrix in Eq. (S58) can be simplified as

$$T_n = \begin{pmatrix} e^{iK} & 0 & 0 & 0 \\ 0 & e^{-ik_n} & 0 & 0 \\ 0 & 0 & e^{ik'_n} & 0 \\ 0 & 0 & 0 & 1 \end{pmatrix}, \quad (\text{S66})$$

So in the limit with $J_0 = 0$, using the transformation of Eq. (S66), we obtain

$$B_4 - A_{14}L = \gamma_0(1 - e^{-iK}), \quad (\text{S67})$$

and the Liouvillian spectral winding becomes

$$W_0 = -\text{Sgn}[\gamma_0] = -1. \quad (\text{S68})$$

IV. AN EXAMPLE WITH CHIRAL-SYMMETRIC QUANTUM JUMPS AND LONGER RANGE HOPPING

We consider a specific Hamiltonian:

$$H = \sum_{l=1}^L (J_0|a, l\rangle\langle b, l| + J_{1,+}|a, l+1\rangle\langle b, l| + J_{1,-}|a, l\rangle\langle b, l+1| + \text{h.c.}), \quad (\text{S69})$$

and jump operators

$$D_{l,0} = \sqrt{\gamma_0}|a, l\rangle\langle b, l|, \quad D_{l,1} = \sqrt{\gamma_1}|a, l+1\rangle\langle b, l|. \quad (\text{S70})$$

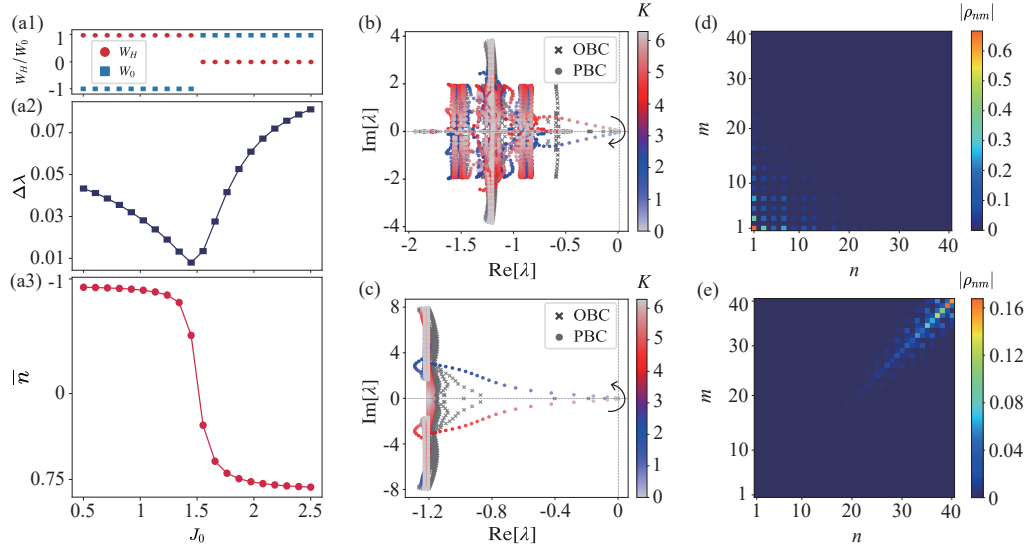


FIG. S1. (a) Topological transition of LSE characterized by the band winding number W_H [red dots in (a1)] and Liouvillian spectrum winding number W_0 [blue squares in (a1)]. Under OBC, the transition manifests as the closing of the Liouvillian gap $\Delta\lambda$ (a2) and the jump of average position \bar{n} of the steady state from one end to the other end of the system. (b) and (c) show the Liouvillian spectrum under OBC (gray) and PBC (colored). Colors represent different K values of the OBC eigenvalues. (d) and (e) the density matrix of the OBC steady-state $\hat{\rho}_0$ in (b) and (c), respectively. (b), (d) have $J_0 = 0.5$, and (c), (e) have $J_0 = 2.5$. The other parameters are $J_{1,+} = 1$, $J_{1,-} = 0.5$, $\gamma_0 = \gamma_1 = 1.2$, and $L = 20$ for OBC.

This Hamiltonian still possesses chiral symmetry:

$$\sigma_z h_c(k) \sigma_z = -h_c(k). \quad (\text{S71})$$

In Fig. S1(a1), we demonstrate the two winding numbers versus J_0 with fixed $J_{1,+}$ and $J_{1,-}$, where the topological transition is seen to occur at $J_0 = J_{1,+} + J_{1,-}$ for both of them. The direction of LSE also changes after crossing this phase transition point [Fig. S1(a3)], accompanied by the Liouvillian gap $\Delta\lambda$ closes [see Fig. S1(a2)]. The complete Liouvillian spectra under PBC and OBC for two representative cases with different winding numbers are shown in Figs. S1(b) and S1(c). The corresponding steady-state density matrices in Figs. S1(d) and S1(e) exhibit LSE in opposite directions.

V. CHIRAL-ASYMMETRIC QUANTUM JUMPS

In this section we derive the Liouvillian spectral winding number under chiral-asymmetric quantum jumps. The asymmetric condition is given by [in contrast to Eq. (S31)]

$$\sigma_z \hat{D}_p \sigma_z = \hat{D}_p, \quad (\text{S72})$$

which allows quantum jumps between the same sublattices, and here we consider those between sublattice a as an example.

We first consider the case with trivial band topology, i.e., $J_s = 0$ for all $s \neq 0$. The Liouvillian superoperator takes the same form as Eqs. (S32) and (S33), with

$$\mathcal{L}(K) = I_L \otimes M + N_L \otimes M_0, \quad (\text{S73})$$

and

$$M = \begin{pmatrix} -B_1 & iJ_0^* & -iJ_0 & 0 \\ iJ_0 & -B_1/2 & 0 & -iJ_0 \\ -iJ_0^* & 0 & -B_1/2 & iJ_0^* \\ 0 & -iJ_0^* & iJ_0 & 0 \end{pmatrix}, \quad M_0 = \begin{pmatrix} A_{11} & 0 & 0 & 0 \\ 0 & 0 & 0 & 0 \\ 0 & 0 & 0 & 0 \\ 0 & 0 & 0 & 0 \end{pmatrix}, \quad (\text{S74})$$

where $A_{11} = \sum_s \gamma_s^{a,a} e^{iKs}/L$, and $B_1 = \sum_{s,\alpha} \gamma_s^{\alpha,a} = \sum_s \gamma_s^{a,a}$, and we have $A_{11}L = B_1$ when $K = 0$. Thus, the eigenvalues of $\mathcal{L}(K)$ (spectrum of M) are given by

$$P_M = \frac{1}{4}(2\lambda + B_1)^2(\lambda^2 + B_1\lambda + 4|J_0|^2) = 0, \quad (\text{S75})$$

which yields

$$\lambda = -\frac{B_1}{2} \quad [\text{multiplicity } 2(L-1)], \quad (\text{S76})$$

$$\lambda = \frac{-B_1 \pm \sqrt{B_1^2 - 16J_0^2}}{2}, \quad [\text{multiplicity } (L-1)]; \quad (\text{S77})$$

and for the spectrum of $M + LM_0$,

$$P_{M+LM_0}(\lambda) = \frac{1}{4}(2\lambda + B_1)P_3(\lambda) = 0, \quad (\text{S78})$$

where

$$P_3(\lambda) = 2\lambda^3 + (3B_1 - 2A_{11}L)\lambda^2 + (B_1^2 + 8|J_0|^2 - B_1A_{11}L)\lambda + 4|J_0|^2(B_1 - A_{11}L), \quad (\text{S79})$$

which yields

$$\lambda = -\frac{B_1}{2} \quad (\text{S80})$$

and the three roots of

$$\lambda^3 + \frac{3B_1 - 2A_{11}L}{2}\lambda^2 + \frac{B_1^2 + 8|J_0|^2 - B_1A_{11}L}{2}\lambda + 2|J_0|^2(B_1 - A_{11}L) = 0, \quad (\text{S81})$$

each with multiplicity 1. Similar to the previous case with $b \rightarrow a$ quantum jumps, the steady state is given by the simple root

$$\lambda_0 = 0 \quad (\text{S82})$$

of Eq. (S81) at $K = 0$, so that $B_1 - A_{11}L = 0$. Upon tuning K slightly away from 0, we have

$$B_1 - A_{11}L = \sum_s \gamma_s^{a,a}(1 - e^{iKs}) \approx -i \sum_s s\gamma_s^{a,a}K, \quad (\text{S83})$$

Thus Eq. (S81) becomes

$$\lambda^3 + \frac{3B_1 - 2A_{11}L}{2}\lambda^2 + \frac{8|J_0|^2 - iB_1 \sum_s s\gamma_s^{a,a}K}{2}\lambda - (2i|J_0|^2 \sum_s s\gamma_s^{a,a})K = 0. \quad (\text{S84})$$

Dropping higher-order terms of $\lambda_0 \sim K$, the perturbed simple root $\lambda_0(K)$ satisfies

$$\lambda_0^3 + \frac{3B_1 - 2A_{11}L}{2}\lambda_0^2 + \frac{8|J_0|^2 - iB_1 \sum_s s\gamma_s^{a,a}K}{2}\lambda_0 - (2i|J_0|^2 \sum_s s\gamma_s^{a,a})K \approx O(\lambda_0^2) + 4|J_0|^2\lambda_0 - (2i|J_0|^2 \sum_s s\gamma_s^{a,a})K = 0, \quad (\text{S85})$$

$$\lambda_0(K) \approx i \sum_s s\gamma_s^{a,a}K. \quad (\text{S86})$$

Alternatively,

$$\lambda_0(K) = \lambda_0(0) - \frac{\partial P_3(\lambda = \lambda_0, K = 0)/\partial K}{\partial P_3(\lambda = \lambda_0, K = 0)/\partial \lambda} + O(K^2) \approx i \sum_s s\gamma_s^{a,a}K. \quad (\text{S87})$$

Therefore we reach the conclusion that the Liouvillian spectral winding corresponds to the winding direction of the complex variant $B_1 - A_{11}L = \sum_s \gamma_s^{a,a}(1 - e^{iKs})$, i.e.,

$$W_0 = \text{Sgn}[\sum_s s\gamma_s^{a,a}]. \quad (\text{S88})$$

Finally, we also consider the case with nontrivial band topology given by a single parameter $J_{s_0} \neq 0$. We can still use the transformation of Eq. (13), but with

$$T_n^{-1}M_0T_n = M_0, \quad (\text{S89})$$

as the only nonzero element of M_0 appears in its diagonal. Therefore, the Liouvillian superoperator takes exactly the same form of Eqs. (S73) and (S74), only with J_0 replaced by J_{s_0} . Thus, the Liouvillian spectral winding number is also given by Eq. (S88). In other words, the nontrivial band topology of the Hamiltonian H does not affect the Liouvillian spectral winding induced by quantum jumps between the same pseudospin components (e.g., $a \rightarrow a$ in the above example).

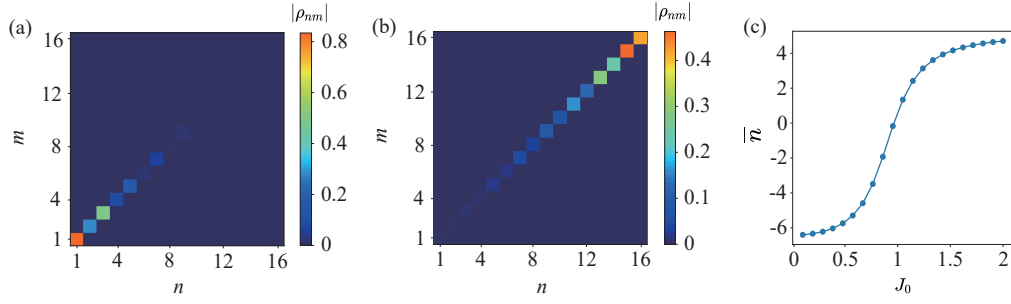


FIG. S2. (a) and (b) reduced density matrix of the steady state with $J_0 = 0.5$ and $J_0 = 2$, respectively. (c) average position of the diagonal terms of density matrix \bar{n} under different J_0 . The other parameters are $J_1 = 1$, $\gamma_0 = \gamma_1 = 1.2$, and $L = 8$.

VI. THE CASE OF TWO HARD-CORE BOSONS.

The creation operator for a hard-core boson is defined as $\hat{c}_{\alpha,l}^\dagger$, which acts on the vacuum state satisfying:

$$\hat{c}_{\alpha,l}^\dagger |0\rangle = |\alpha, l\rangle, \quad (\text{S90})$$

with the additional constraint prohibiting double occupancy:

$$(\hat{c}_{\alpha,l}^\dagger)^2 = 0. \quad (\text{S91})$$

Here, we set nonzero parameter as J_0 , J_1 , $\gamma_0^{a,b} = \gamma_0$, and $\gamma_1^{a,b} = \gamma_1$. In terms of these creation and annihilation operators, the Hamiltonian in Eq.(1) is rewritten as:

$$\hat{H}^{(1)} = \sum_l J_0 \hat{c}_{a,l}^\dagger \hat{c}_{b,l} + J_1 \hat{c}_{a,l+1}^\dagger \hat{c}_{b,l} + \text{h.c.}, \quad (\text{S92})$$

and the jump operators in Eq.(3) is rewritten as:

$$\hat{D}_{l,1}^{a,b} = \gamma_1 \hat{c}_{a,l+1}^\dagger \hat{c}_{b,l}, \quad \hat{D}_{l,0}^{a,b} = \gamma_0 \hat{c}_{a,l}^\dagger \hat{c}_{b,l}. \quad (\text{S93})$$

Based on the description above, we can write the Hamiltonian for two hard-core bosons as:

$$\hat{H}^{(2)} = \hat{P}(\hat{H}^{(1)} \otimes I + I \otimes \hat{H}^{(1)})\hat{P}, \quad (\text{S94})$$

where

$$\hat{P} = \sum_{(\alpha,l) < (\alpha',l')} \hat{c}_{\alpha,l}^\dagger \hat{c}_{\alpha',l'}^\dagger |0\rangle \langle 0| \hat{c}_{\alpha,l} \hat{c}_{\alpha',l'} \quad (\text{S95})$$

is the projection operator. Similarly, the dissipative operator can be written as:

$$\hat{D}_{\alpha,l}^{\alpha,\alpha'(2)} = \hat{P}(\hat{D}_{\alpha,l}^{\alpha,\alpha'} \otimes I + I \otimes \hat{D}_{\alpha,l}^{\alpha,\alpha'})\hat{P}. \quad (\text{S96})$$

Here, we adopt a simpler method to vectorize the density matrix and obtain the form of the Liouvillian superoperator:

$$\mathcal{L} = -i(I \otimes \hat{H}^{(2)} - \hat{H}^{(2)T} \otimes I) + \sum \left(\hat{D}_{\alpha,l}^{\alpha,\alpha'(2)*} \otimes \hat{D}_{\alpha,l}^{\alpha,\alpha'(2)} - \frac{1}{2} I \otimes \hat{D}_{\alpha,l}^{\alpha,\alpha'(2)\dagger} \hat{D}_{\alpha,l}^{\alpha,\alpha'(2)} - \frac{1}{2} (\hat{D}_{\alpha,l}^{\alpha,\alpha'(2)\dagger} \hat{D}_{\alpha,l}^{\alpha,\alpha'(2)})^T \otimes I \right). \quad (\text{S97})$$

Diagonalizing Eq. (S97) yields the steady-state density matrix $\rho^{(2)}$, which is defined on the two-body hard-core boson Hilbert space. To characterize the skin effect distribution in real space more clearly, we further compute the single-particle reduced density matrix:

$$\rho_{(\alpha,l),(\alpha',l')}^{(1)} = \text{Tr}(\rho^{(2)} \hat{c}_{\alpha',l'}^\dagger \hat{c}_{\alpha,l}). \quad (\text{S98})$$

Numerical results for different parameters are presented in Fig.S2. As seen in Fig.S2(a) and (b), when the Hamiltonian is in different topological phases, the LSE exhibits opposite directions, similar to the single-particle case. This is further illustrated by the phase diagram in Fig.S2(c).

† lilinhu@quantumsc.cn

- [1] V. Gorini, A. Kossakowski, and E. C. G. Sudarshan, Completely positive dynamical semigroups of n -level systems, *Journal of Mathematical Physics* **17**, 821 (1976).
- [2] G. Lindblad, On the generators of quantum dynamical semigroups, *Communications in mathematical physics* **48**, 119 (1976).
- [3] C. Gneiting, A. Koottandavida, A. V. Rozhkov, and F. Nori, Unraveling the topology of dissipative quantum systems, *Phys. Rev. Res.* **4**, 023036 (2022).
- [4] D. Paszko, D. C. Rose, M. H. Szymańska, and A. Pal, Edge modes and symmetry-protected topological states in open quantum systems, *PRX Quantum* **5**, 030304 (2024).
- [5] A. Nava, G. Campagnano, P. Sodano, and D. Giuliano, Lindblad master equation approach to the topological phase transition in the disordered su-schrieffer-heeger model, *Phys. Rev. B* **107**, 035113 (2023).
- [6] C.-E. Bardyn, M. A. Baranov, C. V. Kraus, E. Rico, A. İmamoğlu, P. Zoller, and S. Diehl, Topology by dissipation, *New Journal of Physics* **15**, 085001 (2013).
- [7] W. Nie, M. Antezza, Y.-x. Liu, and F. Nori, Dissipative topological phase transition with strong system-environment coupling, *Phys. Rev. Lett.* **127**, 250402 (2021).
- [8] X.-S. Xu, X.-F. Zhou, G.-C. Guo, and Z.-W. Zhou, Dissipation-induced liouville-majorana modes in open quantum system, *Phys. Rev. Res.* **5**, 043004 (2023).
- [9] M. Kawasaki, K. Mochizuki, and H. Obuse, Topological phases protected by shifted sublattice symmetry in dissipative quantum systems, *Phys. Rev. B* **106**, 035408 (2022).
- [10] Z. Gong, Y. Ashida, K. Kawabata, K. Takasan, S. Higashikawa, and M. Ueda, Topological phases of non-hermitian systems, *Phys. Rev. X* **8**, 031079 (2018).
- [11] N. Okuma, K. Kawabata, K. Shiozaki, and M. Sato, Topological origin of non-hermitian skin effects, *Phys. Rev. Lett.* **124**, 086801 (2020).
- [12] K. Zhang, Z. Yang, and C. Fang, Correspondence between winding numbers and skin modes in non-hermitian systems, *Phys. Rev. Lett.* **125**, 126402 (2020).
- [13] F. Koch, Y.-M. Hu, and J. C. Budich, Liouvillian topology and non-reciprocal dynamics in open floquet chains, *arXiv preprint arXiv:2511.16742* (2025).
- [14] F. Song, S. Yao, and Z. Wang, Non-hermitian skin effect and chiral damping in open quantum systems, *Phys. Rev. Lett.* **123**, 170401 (2019).
- [15] T. Haga, M. Nakagawa, R. Hamazaki, and M. Ueda, Liouvillian skin effect: Slowing down of relaxation processes without gap closing, *Phys. Rev. Lett.* **127**, 070402 (2021).
- [16] F. Yang, Q.-D. Jiang, and E. J. Bergholtz, Liouvillian skin effect in an exactly solvable model, *Phys. Rev. Res.* **4**, 023160 (2022).
- [17] S. Hamanaka, K. Yamamoto, and T. Yoshida, Interaction-induced liouvillian skin effect in a fermionic chain with a two-body loss, *Phys. Rev. B* **108**, 155114 (2023).
- [18] L. Mao, X. Yang, M.-J. Tao, H. Hu, and L. Pan, Liouvillian skin effect in a one-dimensional open many-body quantum system with generalized boundary conditions, *Phys. Rev. B* **110**, 045440 (2024).
- [19] X. Li, M. A. Begaowe, S. Zhang, and B. Flebus, Non-hermitian and liouvillian skin effects in magnetic systems, *Phys. Rev. B* **112**, 134416 (2025).
- [20] A. Sannia, G. L. Giorgi, S. Longhi, and R. Zambrini, Liouvillian skin effect in quantum neural networks, *Optica Quantum* **3**, 189 (2025).
- [21] C. Ekman and E. J. Bergholtz, Liouvillian skin effects and fragmented condensates in an integrable dissipative bose-hubbard model, *Phys. Rev. Res.* **6**, L032067 (2024).
- [22] Z. Wang, Y. Lu, Y. Peng, R. Qi, Y. Wang, and J. Jie, Accelerating relaxation dynamics in open quantum systems with liouvillian skin effect, *Phys. Rev. B* **108**, 054313 (2023).
- [23] X. Feng and S. Chen, Boundary-sensitive lindbladians and relaxation dynamics, *Phys. Rev. B* **109**, 014313 (2024).
- [24] D.-H. Cai, W. Yi, and C.-X. Dong, Optical pumping through the liouvillian skin effect, *Phys. Rev. B* **111**, L060301 (2025).
- [25] Y.-M. Hu, Z. Wang, B. Lian, and Z. Wang, Many-body non-hermitian skin effect with exact steady states in the dissipative quantum link model, *Phys. Rev. Lett.* **135**, 260401 (2025).
- [26] M. Z. Hasan and C. L. Kane, Colloquium: topological insulators, *Reviews of modern physics* **82**, 3045 (2010).
- [27] X.-L. Qi and S.-C. Zhang, Topological insulators and superconductors, *Reviews of modern physics* **83**, 1057 (2011).
- [28] C.-K. Chiu, J. C. Teo, A. P. Schnyder, and S. Ryu, Classification of topological quantum matter with symmetries, *Reviews of Modern Physics* **88**, 035005 (2016).
- [29] A. J. Daley, Quantum trajectories and open many-body quantum systems, *Advances in Physics* **63**, 77 (2014).
- [30] L. M. Sieberer, M. Buchhold, and S. Diehl, Keldysh field theory for driven open quantum systems, *Reports on Progress in Physics* **79**, 096001 (2016).
- [31] Supplemental materials.
- [32] D. S. Borgnia, A. J. Kruchkov, and R.-J. Slager, Non-hermitian boundary modes and topology, *Phys. Rev. Lett.* **124**, 056802 (2020).
- [33] W. P. Su, J. R. Schrieffer, and A. J. Heeger, Solitons in polyacetylene, *Phys. Rev. Lett.* **42**, 1698 (1979).
- [34] D. Jaksch and P. Zoller, Creation of effective magnetic fields in optical lattices: the hofstadter butterfly for cold neutral atoms, *New Journal of Physics* **5**, 56 (2003).
- [35] M. Aidelsburger, M. Atala, M. Lohse, J. T. Barreiro, B. Paredes, and I. Bloch, Realization of the hofstadter hamiltonian with ultracold atoms in optical lattices, *Phys. Rev. Lett.* **111**, 185301 (2013).
- [36] H. Miyake, G. A. Siviloglou, C. J. Kennedy, W. C. Burton, and W. Ketterle, Realizing the harper hamiltonian with laser-assisted tunneling in optical lattices, *Phys. Rev. Lett.* **111**, 185302 (2013).
- [37] J. Dalibard and C. Cohen-Tannoudji, Atomic motion in laser light: connection between semiclassical and quantum descriptions, *Journal of Physics B: Atomic and Molecular Physics* **18**, 1661 (1985).
- [38] H. Pichler, A. J. Daley, and P. Zoller, Nonequilibrium dynamics of bosonic atoms in optical lattices: Decoherence of many-body states due to spontaneous emission, *Phys. Rev. A* **82**, 063605 (2010).
- [39] J. F. Poyatos, J. I. Cirac, and P. Zoller, Quantum reservoir engineering with laser cooled trapped ions, *Phys. Rev. Lett.* **77**, 4728 (1996).
- [40] P. M. Harrington, E. J. Mueller, and K. W. Murch, Engineered dissipation for quantum information science, *Nature Reviews Physics* **4**, 660 (2022).
- [41] X. Mi, A. Michailidis, S. Shabani, K. Miao, P. Klimov, J. Lloyd, E. Rosenberg, R. Acharya, I. Aleiner, T. Andersen, *et al.*, Stable quantum-correlated many-body states through engineered dissipation, *Science* **383**, 1332 (2024).